

# DH-PTAM: A Deep Hybrid Stereo Events-Frames Parallel Tracking And Mapping System

Abanob Soliman , Fabien Bonardi , Désiré Sidibé , and Samia Bouchafa 

**Abstract**—This paper presents a robust approach for a visual parallel tracking and mapping (PTAM) system that excels in challenging environments. Our proposed method combines the strengths of heterogeneous multi-modal visual sensors, including stereo event-based and frame-based sensors, in a unified reference frame through a novel spatio-temporal synchronization of stereo visual frames and stereo event streams. We employ deep learning-based feature extraction and description for estimation to enhance robustness further. We also introduce an end-to-end parallel tracking and mapping optimization layer complemented by a simple loop-closure algorithm for efficient SLAM behavior. Through comprehensive experiments on both small-scale and large-scale real-world sequences of VECtor and TUM-VIE benchmarks, our proposed method (DH-PTAM) demonstrates superior performance compared to state-of-the-art methods in terms of robustness and accuracy in adverse conditions. Our implementation’s research-based Python API is publicly available on GitHub for further research and development: <https://github.com/AbanobSoliman/DH-PTAM>.

**Index Terms**—Stereo, events, SuperPoint, R2D2, SLAM.

## I. INTRODUCTION

**S**ENSOR fusion [1] combines data from multiple sensors to improve a system’s accuracy, reliability, and robustness. It can also reduce computational costs by eliminating the need for redundant sensor data. Different types of sensors can be fused, such as cameras, lidars, radars, and ultrasonics. The algorithm used for fusion can vary, and it typically requires online calibration to ensure accurate and consistent data.

Visual Odometry (VO) is a method that utilizes sensor fusion to estimate the motion of a camera by analyzing the changes in visual features between consecutive frames. Still, it faces challenges, such as difficulties in feature matching when the scene has little texture, the need for a robust feature detector and descriptor, and the problems of relative scale ambiguity and drift [2]. Scale ambiguity refers to the problem of determining the actual scale of the scene. In contrast, drift refers to the accumulation of errors over time that causes the estimated positions to deviate from the true positions. These challenges and limitations must be considered when applying frame-based visual odometry in practical applications [3].

An event camera [4], known as an asynchronous or dynamic vision sensor (DVS), operates on a fundamentally different concept than traditional frame-based cameras. Instead of capturing frames at a constant rate, event cameras output a stream of “events” that indicate the brightness changes in each pixel. This allows event cameras to operate at high speed, in very low-light conditions, and be more resistant to motion blur [5].

The event-based nature of these cameras also makes them highly suitable for tasks that involve fast-moving objects or scenes with high dynamic range. These characteristics make them an excellent complementary sensor to frame-based visual odometry in adverse conditions such as fast motion, high dynamic range, and low-light environments, where traditional cameras may struggle.

Deep learning-based features are more robust than traditional methods [6], [7], as they can learn from large amounts of data and generalize well to unseen data. They are also more invariant to changes in viewpoint and lighting, making them suitable for real-world applications. Recently, pre-trained models have been widely adopted in computer vision and have achieved state-of-the-art performance in object detection, semantic segmentation, and image classification tasks.

In this paper, we propose a deep hybrid stereo events-frames parallel tracking and mapping system that significantly improves simultaneous localization and mapping accuracy and robustness in dynamic environments. This system combines the advantages of stereo RGB and event cameras, which can capture visual information at high temporal resolution. The use of deep learning techniques in this system allows for the extraction of robust features from the stereo hybrid image and event frames, which improves the accuracy of the feature-matching process and the estimation of the camera pose.

Our main contributions can be summarized as follows:

- We propose an end-to-end parallel tracking and mapping (PTAM) approach based on a novel spatio-temporal synchronization of stereo visual frames with event streams (see Fig. 1).
- We propose a simple mid-level feature loop-closure algorithm for prompt SLAM behavior based on a learning-based feature description method to maximize robustness.
- DH-PTAM’s effectiveness is evaluated in both stereo event-aided and image-based visual SLAM modes, achieving improved accuracy when incorporating event information, shown in an ablation study on the CPU versus the GPU of a consumer-grade laptop.

This paper is organized as follows: Section II gives a brief overview of the state-of-the-art SLAM methods. Section III provides an in-detail overview of the proposed method and offers insights of the novel parts of the algorithm. Section IV comprehensively evaluates the algorithm on the most recent VECtor [8] and TUM-VIE [9] benchmarks, along with defining the limitations. Section V summarizes the experiments’ main observations, the proposed method’s behavioral aspects, and the start points for future works.

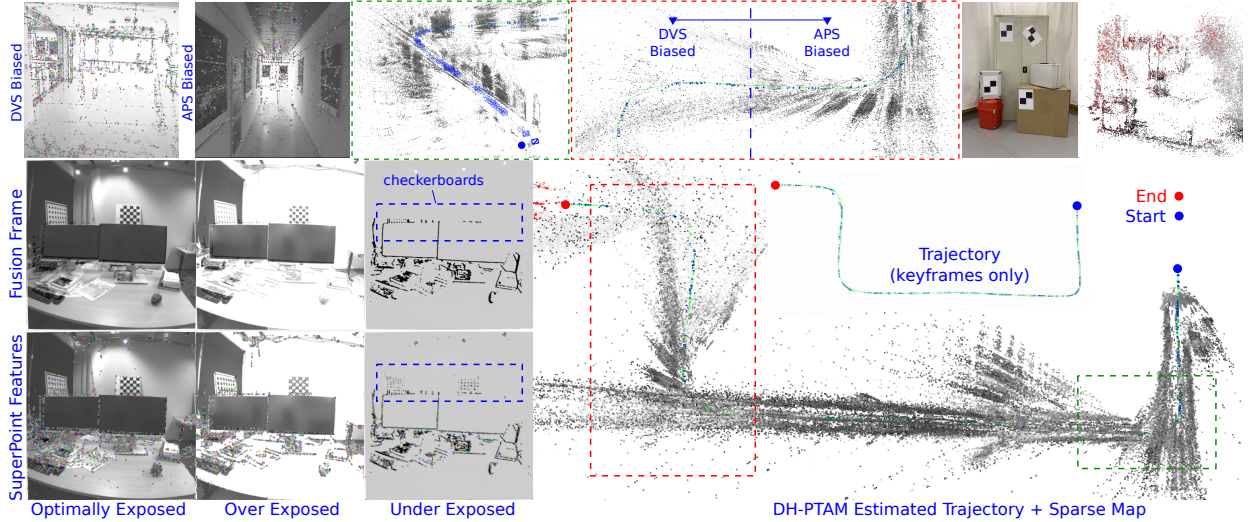


Fig. 1. Top & Bottom (right): snippets of experiments on school-scooter and corner-slow sequences from the VECtor dataset that show the estimated trajectory with the constructed scene map (green dotted rectangle). Red dotted rectangle highlights an HDR use-case where DH-PTAM estimates the trajectory continuously based on the two fusion modes (Dynamic Vision Sensor (DVS) or Active Pixel Sensor (APS) biased). Bottom (left): snippets of an experiment on a small-scale (mocap-desk2) sequence from the TUM-VIE dataset that show the capability of the proposed events-frames fusion method to maintain and track features in dimmed and bright scenes where grayscale-only frames fail. APS: denotes the standard camera’s global shutter frames.

## II. RELATED WORK

### A. Conventional visual-SLAM

Simultaneous Localization and Mapping (SLAM) problem has been widely studied in the literature [10], and various techniques have been proposed to solve it. In recent years, learning-based features extraction and description methods [6], [7], and deep learning based approaches [11] have been applied to improve SLAM robustness.

One of the most popular SLAM techniques is the filter-based SLAM using an extended Kalman filter (EKF) [1], or a particle filter [12]. These filters use probabilistic frameworks to estimate the robot’s pose and map. They can handle non-linearities and uncertainties in the system, making them useful for large-scale and highly dynamic environments. Filter-based SLAM has been widely used in applications [13] such as mobile robots, UAVs, and autonomous vehicles.

Another important class of SLAM is graph-based SLAM [14], which uses a factor graph data structure to represent the robot’s poses and the map. Graph-based SLAM requires Sparse Bundle Adjustment (SBA), which uses a non-linear least squares optimization to estimate the robot’s poses and a graph to represent the map. These methods are robust to changes in lighting and viewpoint, making them well-suited for real-world applications. Some popular graph-based SLAM methods include ORB-SLAM [15], Basalt [16], and VINS-Fusion [17].

Loop-closure detection is a fundamental approach to minimize drifts in visual-SLAM, as it allows a system to recognize a previously visited location. Two common approaches to loop-closure detection are mid-level features [18] and bag-of-words [19] representations. Mid-level features are more abstract than low-level features, such as edges and corners, but are not as high-level as object recognition. Deep learning descriptors [20] can be considered mid-level features as they

can extract higher-level information from raw data compared to low-level features, such as pixel values, but are not as high-level as features directly related to the task at hand, such as object labels.

### B. Event-aided visual-SLAM

Event-based VO is an emerging form of localization solution that uses event-based cameras to generate measurements of the environment. While the number of sampled frames limits traditional SLAM, event-based SLAM provides high temporal resolution by generating an abundance of measurements, allowing for improved 3D localization and 6D pose estimation. Indirect methods, such as frame-based approaches, extract keypoints from the input data in the front-end. This front-end stage typically involves detecting and matching salient features in the sensory data, such as images or event streams. These keypoints are then passed to the back-end, where state estimation algorithms are used to estimate the robot’s pose and build a consistent map of the environment.

Conversely, direct methods attempt to process all available sensor data, such as individual pixel intensity changes in images (events) or all RGB frame pixels, without any intermediate filtering or feature extraction in the front-end, relying on the back-end to handle the entire data.

Event-aided systems leverage the high-quality representations that events can produce after processing, especially in dynamic and dimmed environments where RGB camera frames fail. Some of the well-known event representations are event image (EI) [21], Time Surfaces (TS) [22], Event Spike Tensor (EST) [23], and recently Event 3-Channel Tensor (E3CT) [24]. Others [4] build the front-end on an Event Generation Model (EGM) [25] or construct motion-compensated event frames (MEF) [26] aided by a gyroscope. Towards a traditional frame reconstruction from events, [27] proposes a

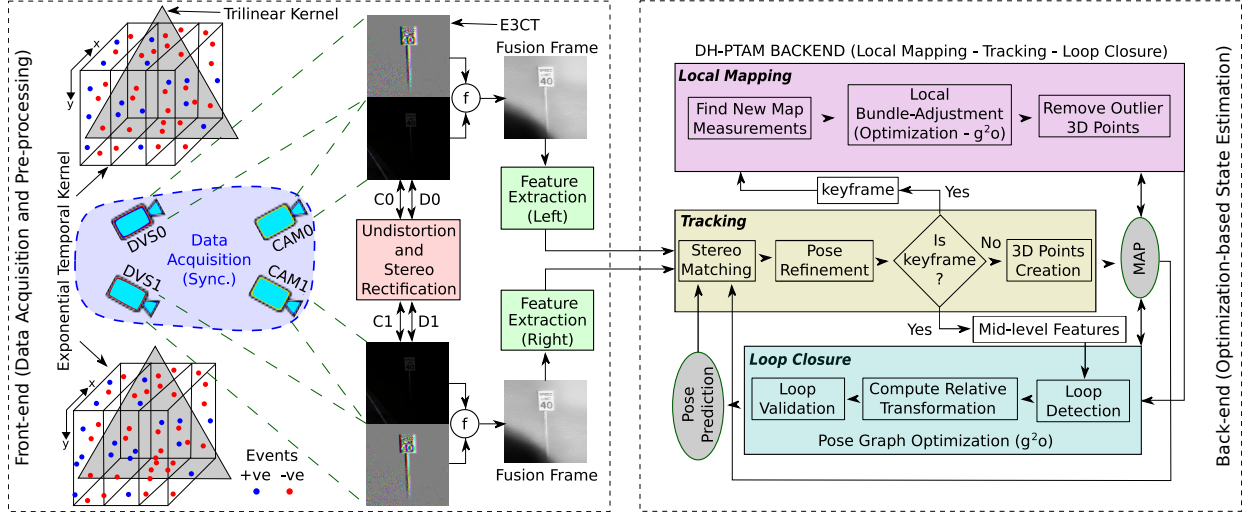


Fig. 2. Block diagram of the proposed event-aided hybrid stereo odometry approach (DH-PTAM). DVS denotes "Dynamic Vision Sensor" (event camera).

Log Intensity Reconstruction (LIR), a model-based method, and [28] proposes Spade-e2vid, a learning-based method.

Table I compares the latest event-based and event-aided VO solutions concerning the sensor setup, events pre-processing layer (EPL), direct or indirect event processing, and the loop-closure capability to minimize visual drifts.

TABLE I  
DIRECT AND INDIRECT (D/I) VISUAL ODOMETRY METHODS BASED (B) ON EVENTS AND/OR AIDED (A) BY EVENTS

Method	B/A	D/I	EPL <sup>a</sup>	LC <sup>b</sup>	More Information
Kim [27]	B	D	LIR	×	3 EKFs + Image reconst.
Rebecq [21]	B	D	EI	×	Monocular (PTAM)
Zhou [29]	B	D	TS	×	Stereo (PTAM)
Kueng [30]	A	I	×	×	Event-aided Tracking
Rosinol [26]	A	I	MEF	×	Mono + IMU (front-end)
Hidalgo-Carrió [4]	A	D	EGM	×	Monocular Odometry
<b>Proposed</b>	A	I	E3CT	✓	Stereo (PTAM) + DL <sup>c</sup>

<sup>a</sup> denotes an Event Pre-processing Layer. <sup>b</sup> denotes Loop-Closure capability. <sup>c</sup> denotes the only method incorporating Deep Learning-aided features.

### III. METHODOLOGY

#### A. System Overview

Fig. 2 illustrates the main components and the process of DH-PTAM. The system establishes a global reference frame based on the camera position in the initial frame. A preliminary map is created by identifying and triangulating distinctive points in the first stereo pair of images. For subsequent frames, the tracking thread calculates the 6D pose of each stereo frame by minimizing the discrepancy between the projected map points and their matches. The system chooses a subset of keyframes used in another thread to update the map at a slower pace.

Map points are derived from the stereo matches of each keyframe and added to the map. The mapping thread constantly improves the local discrepancy by adjusting all map points, and stereo poses using Bundle Adjustment. A pose graph is utilized to preserve the global consistency of the

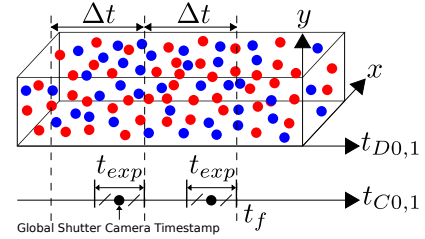


Fig. 3. Spatio-temporal synchronization scheme.  $t_{exp}$  is the global shutter camera exposure time.  $\Delta t$  is the event representation (E3CT) volume accumulation time.  $t_f$  is the fusion frame calculated timestamp.  $t_{D,C}$  are the DVS events, and RGB camera frames timestamps, respectively.

map which is a shared resource among the tracking, mapping, and loop-closing threads. Point correspondences are actively searched between keyframes to strengthen the constraints of the pose graph optimization smoothing process.

**Notations.** The odometry state representation comprises the 3D points  $X_w^k$  and a 7-increment vector  $\mu \in \mathfrak{se}(3)$ , which is the current pose of the left fusion frame at time  $k$ :

$$\mu^k = [\delta x \ \delta y \ \delta z \ \delta q_x \ \delta q_y \ \delta q_z \ \delta q_w]^\top, \quad (1)$$

where  $[\delta x \ \delta y \ \delta z]^\top$  is the incremental translation vector and  $[\delta q_x \ \delta q_y \ \delta q_z \ \delta q_w]^\top$  is the incremental quaternion vector.

#### B. Spatio-temporal Synchronization

Our spatio-temporal synchronization approach (see Fig. 3) considers the general case of global shutter cameras where the exposure time  $t_{exp0,1}$  is known. We adopt the constant-time  $\Delta t_{0,1}^k$  events accumulation window  $k$  approach in our spatio-temporal events-frames synchronization method.

As soon as stereo RGB camera frames are received at timestamps  $t_{C0,1}$ , we calculate the fusion frames timestamps assuming the hardware synchronization of stereo RGB images and stereo event streams, using:

$$t_{f0,1} = t_{C0,1} + \frac{t_{exp0,1}}{2}, \quad \Delta t_{0,1}^k = t_{f0,1}^k - t_{f0,1}^{k-1}, \quad (2)$$



where  $t_{C_0}$  is the selected stereo keyframe timestamp.

### C. Events-Frames Hybridization Approach

One of the main advantages of our front-end fusion modeling is that it does not rely on any online probabilistic photometric matching or alignment approach using filters or cost functions and considers all events polarities  $p \in \{+1, -1\}$ . Hence, the computational load of our method lies mainly on the PTAM modules of the optimization-based back-end. The E3CT events pre-processing layer is adopted and modeled as two consecutive filtering kernel convolutions on the event volume  $\mathcal{V}_0(x, y, t)$  of temporal width  $\Delta t_{0,1}^k$ . The first kernel to filter the time decaying events in the volume, is the  $\alpha$ -exponential time decay kernel and is modeled as:

$$\mathcal{V}_1(x, y, t) \doteq \exp \left( -\alpha \left( \frac{\mathcal{V}_0(x, y, t) - \eta/2}{\eta/6} \right)^2 \right), \quad (3)$$

where  $\alpha = 0.5$  and the decay rate  $\eta = 30$  [ms] for our model. Followed by a trilinear voting kernel to stack the events in the three channels tensor so that each event contributes to two consecutive channels depending on their location from a vertex of this trilinear kernel. An event near the top contributes a higher weight to the current channel and a lower weight to the neighboring ones. These contribution weights of the three channels can represent a percentage of an R-G-B color map; hence, the E3CT can be considered a synthetic RGB frame of events. The trilinear voting kernel can be modeled as follows:

$$\mathcal{V}_2(x, y, t_i) \doteq \max \left( 0, 1 - \left| \frac{\mathcal{V}_1(x, y, t_i)}{\delta t} \right| \right), \quad (4)$$

where  $\delta t$  is the temporal bin  $i$  size as discussed in [23].

After applying the trilinear temporal voting kernel on the exponential-decay time surface, we stack the 3-channel tensor temporal bins together, resulting in a synthetically colored 2D frame called the Event 3-Channel Tensor (E3CT). In Fig. 2, we can observe that the constructed synthetic colors are always consistent, meaning that the stereo left and right constructed E3CTs have identical colors for the same scene.

Conventional frame-based post-processing operations can be applied to the constructed E3CTs, such as adaptive threshold, contrast stretching, color correction and balance, and denoising functions. We consider a fully calibrated stereo RGB and event cameras stack as represented in Fig. 4, so that the rigid-body transformations  $\mathcal{T}_{cd_{0,1}} = [R_{cd_{0,1}} | t_{cd_{0,1}}]_{3 \times 4}$  and the cameras intrinsic parameters  $\mathcal{K}_{c_{0,1}}, \mathcal{K}_{d_{0,1}}$  are known.

Given that the same post-processing operations are applied on the current stereo E3CT frames, the 2D-to-3D-to-2D consecutive inverse-forward projections of the pixels on the E3CT frames  $P_{d_{0,1}}^h$  to the RGB camera frames  $P_{d \in c_{0,1}}^h$  can be performed as follows:

$$P_{d \in c_{0,1}}^h \approx \mathcal{K}_{c_{0,1}} \mathcal{T}_{cd_{0,1}} [(\mathcal{K}_{d_{0,1}})^{-1} P_{d_{0,1}}^h \quad 1]^\top + \delta P_{align}^h, \quad (5)$$

where  $(\cdot)^h$  denotes the pixel location in homogeneous coordinates. The term  $\delta P_{align}^h$  denotes the pixel location alignment correction factor for the RGB and event frames (see Fig. 5)

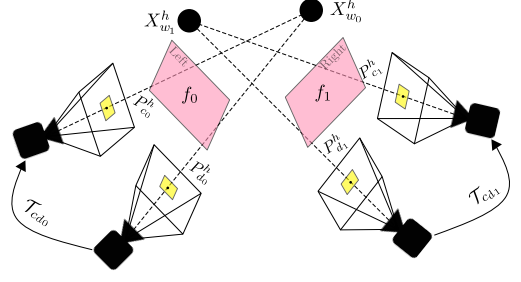


Fig. 4. Geometry of the stereo hybrid event-RGB cameras stack.

so that the same 3D world point  $X_{w0,1}^h$  should correspond exactly to the pixel locations  $P_{d \in c_{0,1}}^h, P_{c_{0,1}}^h$ . This alignment term is observed to be constant for the same sensor rig with non-varying intrinsic and extrinsic parameters.  $\delta P_{align}^h$  value can be estimated using an offline optimization process only once on a selected number of frames (the more the accurate) with high confidence feature matches, and this value is given in Section IV for both VECtor and TUM-VIE sequences.

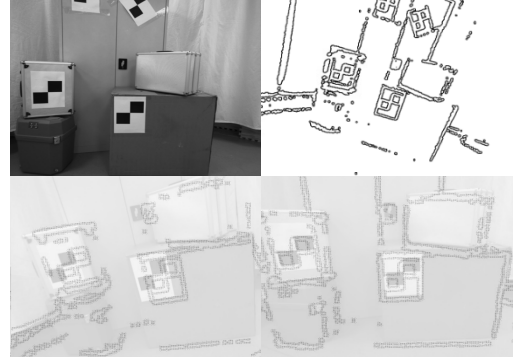


Fig. 5. E3CT alignment with the RGB camera frame. Top: RGB camera frame (left) and E3CT post-processed frame (right). Bottom: E3CT-RGB camera fusion frames before (left) and after (right)  $\delta P_{align}^h$  correction.

Finally, the fusion function (and frame)  $f(\cdot)$  performs a temporal cross-dissolve (linear blending) between both the left ( $D_0, C_0$ ) and right ( $D_1, C_1$ ) E3CTs and RGB camera frames, respectively, and is formulated as:

$$f_{0,1}(C_{0,1}, D_{0,1}) = (1 - \beta) * C_{0,1} + \beta * D_{0,1}, \quad (6)$$

where  $\beta \in [0, 1]$  is the E3CT contribution weight in the current fusion frame.  $\beta$  value is dynamic and depends on the scene lighting and texture conditions. It should be set to high values  $\beta = \max(\frac{C_{0,1}}{C_{0,1}^{max}}, 1 - \frac{C_{0,1}}{C_{0,1}^{max}})$  when the RGB camera frame fails to detect features due to adverse conditions and low-textured scenes, and this is the DVS-biased fusion mode. For situations where RGB camera frames can detect reliable scene features with good lighting and enough texture, the  $\beta$  value should be low  $\beta = \min(\frac{C_{0,1}}{C_{0,1}^{max}}, 1 - \frac{C_{0,1}}{C_{0,1}^{max}})$  to reduce the amount of extracted features and maintain the back-end processing complexity and latency in reasonable ranges, and this is the APS-biased fusion mode.

Dynamic scenes with challenging and adverse conditions can easily trigger rapid switching between these two fusion



modes during long-term navigation. This causes a critical problem during the feature tracking process using conventional low-level feature detectors, such as ORB, SIFT, SURF, BRIEF, and FAST. Accordingly, applying mid-level feature detectors that depend mainly on learning-based architectures could solve this fusion frame modes alternation problem. We employ the learning-based feature extractors and descriptors [6], [7] for their high robustness and feature detection speed. In Fig. 6, we notice the stable tracking of the learning-based features on the hybrid fusion frames in this high dynamic range scenario.

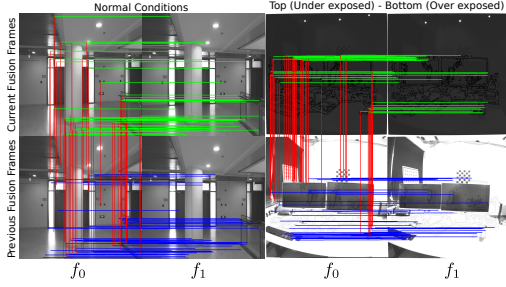


Fig. 6. Spatio-temporal matching for SuperPoint features on two consecutive stereo fusion frames. A random batch of 50 matches is selected as a sample.

#### D. Optimization-based State Estimation

As our work is based on the original S-PTAM system, all the optimization Jacobians mentioned in this section can be found with detailed proofs in [31]. All objective functions are minimized with the Levenberg-Marquardt algorithm implemented in the  $g^2o$  optimization library. We employ the Huber loss function for outliers rejection  $\rho(\cdot)$ .

**System bootstrapping.** The first stereo fusion frames are considered a keyframe. Then, a triangulation for the collected feature matches on the left and right fusion frames is performed to initialize the map.

**Pose tracking thread.** Each map point is projected into the viewing frustum of the anticipated stereo position, and we then look nearby for the match. A valid prediction of the current pose is required for such a projection. By contrasting the descriptions, map points and features are matched. The  $L_2$  norm is computed using the binary descriptors of SuperPoint and R2D2. The match is valid if the distance falls below a certain threshold; otherwise, it is ignored. The pose refinement is then applied to recover the current pose knowing the previous one using the following objective function:

$$L^{\text{refine}} = \arg \min_{\mu} \sum_{i \in N} \rho(\|J_i^k \mu_k - \Delta z_i(\mu_{k-1}, X_w^i)\|^2), \quad (7)$$

where  $N = \{z_1, \dots, z_M\}$  and  $M$  is the number of matched measurements. The measurement  $z = [u, v]^T$  is a pixel 2D location of the forward projection of a 3D map point  $X_w$  using the pinhole model projection function  $\pi(X_w^i) = \mathcal{K}_c \mathcal{T}_i^{f_0w} X_w^i$ .  $J_i^k = \frac{\partial \Delta z_i(\mu)}{\partial \mu_k}$  is the re-projection error's Jacobian with respect to the current odometry state vector.  $\Delta z$  is the re-projection error of a matched set of measurements on the current  $k$  stereo fusion frames and is defined as:

$$\Delta z_i(\mu, X_w) = z_i - \pi(\exp(\mu) \mathcal{T}_{k-1}^{f_0w} X_w^i), \quad (8)$$

where the 3D point cloud  $X_w$  is considered a constant optimization parameter and not updated in the tracking thread and  $\mathcal{T}_{k-1}^{f_0w} = \exp(\mu) \in SE(3)$  with  $\exp(\cdot)$  the exponential map in the  $SE$  group for the previous increment state vector. If the number of observed points is less than 90% of the points recorded in the previous keyframe, a frame is chosen to be a keyframe after the current pose has been evaluated. Then, new map points are created by triangulating the stereo pair's remaining mismatched features. The keyframe is then placed in the local mapping thread for processing.

**Mapping thread.** We apply Bundle Adjustment (BA) to fine-tune the camera poses (keyframe map) and the 3D points (point cloud map). Local Bundle Adjustment minimizes the re-projection error of every point in every keyframe  $f_0^k$ . Given an initial set of  $N$  keyframe poses  $\{\mathcal{T}_1^{f_0w}, \dots, \mathcal{T}_N^{f_0w}\}$ , an initial set of  $M$  3D points  $X_w^i$ , and measurement sets  $S \in \{S_1, \dots, S_N\}$ , where each set comprises the measurement  $z_i^k$  of the  $i^{th}$  point in the  $k^{th}$  keyframe, the local BA is performed using the following objective function on all keyframes in a pre-defined sliding-window size  $N$ :

$$L^{\text{BA}} = \arg \min_{\mu, X_w} \sum_{k=1}^N \sum_{i \in S_k} \rho(\|J_i^k \begin{bmatrix} \mu_k \\ X_w^i \end{bmatrix} - \Delta z_i(\mu_k, X_w^i)\|^2), \quad (9)$$

where the 3D point cloud  $X_w$  is considered a variable optimization parameter and is updated in the mapping thread. Hence, the  $J_i^k = [\frac{\partial \Delta z_i(\mu_k, X_w^i)}{\partial \mu_k}, \frac{\partial \Delta z_i(\mu_k, X_w^i)}{\partial X_w^i}]$  is the re-projection error's Jacobian with respect to the current odometry state vector and the 3D point as well.

**Loop-closure thread.** Instead of the conventional way of keyframe embedding assignments using a bag-of-words, we adopt a simple loop-closure detection method based on the mean of the mid-level learning-based feature descriptors (SuperPoint and R2D2) for each keyframe and assign this mean value as the embedding identity of each keyframe. Once a potential loop closure is detected, the system performs geometric verification through RANSAC-based pose estimation to validate the candidate. If the verification is successful, a loop closure constraint is added to the pose graph, and a graph optimization is performed to distribute the error and update the global map, thus correcting the accumulated drift.

## IV. EVALUATION

We perform a thorough, comprehensive evaluation during navigation in real-world, large-scale, and small-scale areas in challenging settings. In subsection IV-A, we compare DH-PTAM with other RGB image-based and event-based/aided methods on the HDR large-scale sequences of the publicly available dataset VECtor [8] due to its high-quality ground truth values and sensors calibration parameters. In subsection IV-B, we evaluate the small-scale (mocap-) sequences of TUM-VIE [9] to test the quality of the DH-PTAM spatio-temporal synchronization method with degraded event camera calibration parameters. Moreover, the first 45 frames

TABLE II

DH-PTAM QUANTITATIVE COMPARISON AGAINST THE BEST PERFORMING OPEN-SOURCE STATE-OF-THE-ART SLAM SYSTEMS USING ATE [M] METRIC. THE UPPER SUB-TABLE IS FOR STANDARD STEREO VIO METHODS, THE MIDDLE IS FOR EVENT-BASED VO/VIO METHODS, AND THE LOWER IS FOR DH-PTAM WITH RPE [M] METRIC. **BOLD** DENOTES BEST PERFORMING, UNDERLINE FOR SECOND BEST PERFORMING, AND (×) DENOTES FAILURE

Method	VECTor sequences [8]						TUM-VIE sequences [9]					Mean VECTor large-scale	Mean TUM-VIE small-scale
	corridors dolly	corridors walk	units dolly	units scooter	school dolly	school scooter	mocap 1d-trans	mocap 3d-trans	mocap 6dof	mocap desk	mocap desk2		
ORB-SLAM3 (SVIO) [15]	<b>0.802</b>	<u>1.031</u>	18.063	14.504	<b>0.921</b>	<u>0.752</u>	<u>0.007</u>	0.012	0.018	<b>0.007</b>	0.025	6.012	<u>0.013</u>
BASALT (SVIO) [16]	1.625	2.152	11.151	13.256	1.852	1.482	<b>0.003</b>	0.009	<b>0.014</b>	0.016	<u>0.011</u>	5.253	<b>0.011</b>
VINS-Fusion (SVIO) [17]	1.464	<b>0.392</b>	10.391	11.471	1.791	<b>0.562</b>	0.011	0.011	<u>0.017</u>	0.058	0.013	4.345	0.022
EVO (Mono Events) [21]	×	×	×	×	×	×	0.075	0.125	0.855	0.541	0.752	×	0.470
ESVO (Stereo Events) [29]	×	×	×	×	13.710	9.830	0.009	0.028	0.058	0.033	0.032	11.77	0.032
Ultimate SLAM (EVIO) <sup>+</sup> [26]	×	×	×	×	×	6.830	0.039	0.047	0.353	0.195	0.341	6.830	0.195
<b>DH-PTAM (Stereo Fusion)</b>	1.884	1.299	<b>5.274</b>	<u>8.433</u>	<u>1.093</u>	0.796	0.103	<u>0.007</u>	0.024	0.016	0.015	<u>3.130</u>	0.033
(SuperPoint on CPU) - RPE ( $\sigma$ )	0.073	0.038	0.055	0.149	0.178	0.074	0.006	<b>0.007</b>	0.009	0.009	0.007	0.095	0.008
<b>DH-PTAM* (Stereo Image)</b>	1.841	1.543	<u>5.738</u>	<b>5.010</b>	1.559	0.877	0.099	<b>0.004</b>	0.045	<u>0.011</u>	<b>0.008</b>	<b>2.761</b>	0.033
(R2D2 on GPU) - RPE ( $\sigma$ )	0.116	0.141	0.134	0.308	0.202	0.331	0.014	0.020	0.022	0.023	0.021	0.205	0.020

<sup>+</sup> IMU sensor is included since it is integrated into the front-end and cannot be separated for a fair comparison with EVO, ESVO, and DH-PTAM (ours).

\* in this ablation case study, the SuperPoint detector is replaced with the R2D2 detector (trained for SLAM tasks), leveraging the GPU performance.

TABLE III  
DH-PTAM PARAMETERS CONFIGURATION

Parameter	VECTor sequences	TUM-VIE sequences
$\delta P_{align}^h$ - Left	(-160, -235) [px]	(355, 40) [px]
$\delta P_{align}^h$ - Right	(-160, -235) [px]	(375, 45) [px]
frustum_near	0.1 [m]	0.1 [m]
frustum_far	30.0 [m]	5.0 [m]
matching_cell_size	15 [px]	15 [px]
matching_neighborhood	2 [px]	1.8 [px]
matching_distance	25 [px]	15 [px]

TABLE IV  
COMPUTATIONAL COMPLEXITY ANALYSIS ON CPU VS. GPU

Thread	#Tasks	Operation	CPU [ms]	GPU [ms]
Front-end	3	Stereo E3CT Construction	25-30	76-172
		Events-Frames Fusion	439-521	191-352
Bootstrapping	( $\approx 2 \times 10K$ )	SuperPoint Detection	2478-3256	521-1752
	( $\approx 2 \times 4K$ )	R2D2 Detection	8532-8752	1067-2254
Tracking	1	Initialize the Map	106-143	53-120
	2	Spatio-temporal Matching	161-215	142-172
Mapping	(10 iter.)	Pose Refinement	11-15	10-12
	2	Update Map	1-3	0.452-1
Loop-closing	(30 iter.)	Local Bundle-Adjustment	1-4	1-2
	3	Loop Detection	14-20	10-15
		Compute and Validate	2-5	1-3
	(30 iter.)	Pose Graph Optimization	1-3	0.524-2
End-to-End	11	SuperPoint Detector	3153-4208	356-1962
		R2D2 Detector	8560-9125	1226-2486

of TUM-VIE sequences suffer a high over-/under-exposure global shutter alternation, which tests the DH-PTAM's pose estimation stability. We perform a comparative quantitative analysis to evaluate the accuracy of our system in Table II and a qualitative/quantitative analysis in Fig. 7. The accuracy of DH-PTAM is measured with absolute trajectory error (ATE), and relative pose error (RPE) metrics calculated using the baseline SLAM evaluation tool [32].

To prevail the advantages of complementing the sensor stack with events information, we compare our event-aided stereo visual odometry solution (DH-PTAM) to the latest best-performing open-source visual-inertial systems in literature in Table II. Table III gives the system parameters configuration for large-scale and small-scale sequences. We keep these parameters constant for all sequences of the same scale group without an online fine-tuning process.

All experiments are performed on the CPU and the GPU of a 16 GB RAM laptop computer running 64-bit Ubuntu 20.04.3 LTS with AMD(R) Ryzen 7 4800h  $\times 16$  cores 2.9 GHz processor and a Radeon RTX NV166 Renoir graphics card. Table IV reports a detailed computational complexity analysis for our DH-PTAM system with minimal and maximal system requirements. The high CPU load observed when detecting SuperPoint and R2D2 features can be attributed to the algorithms' design, which prioritizes feature quality and robustness over computational efficiency. This trade-off is often necessary for computer vision research, where high-quality results are crucial for many applications but come at the cost of increased computational complexity. The back-end

runs with real-time performance, and it is recommended to run the front-end on a GPU to achieve a memory efficient, faster, and more stable performance.

**No event streams** ( $\beta = 0$ ). In Table II, we show an ablation study where we run DH-PTAM on stereo images. We notice estimation failure with all the conventional and learning-based feature detectors except R2D2. Although the ATE metric shows slightly better results without using events, the RPE metric shows much more accurate values when using events. These better ATE values are due to the high performance of the GPU in loop-closures using R2D2 features (see Fig. 7).

#### A. VECTor large-scale experiments

We notice a prominent estimation failure in Table II while evaluating the event-based methods EVO, ESVO and Ultimate SLAM on the large-scale sequences. Numerous factors may contribute to the failure of these systems, including stringent initialization requirements. For instance, the system EVO necessitates running in a sensor-planar scene for several seconds to bootstrap the system. Additionally, these systems are susceptible to parameter tuning, as demonstrated by using different parameters for different sequences in the same scenarios, even within their open-source projects.

Table II shows a good performance for DH-PTAM compared to the competing VI-SLAM systems. Although Fig. 7 shows high visual drifts for our vision-only system in the

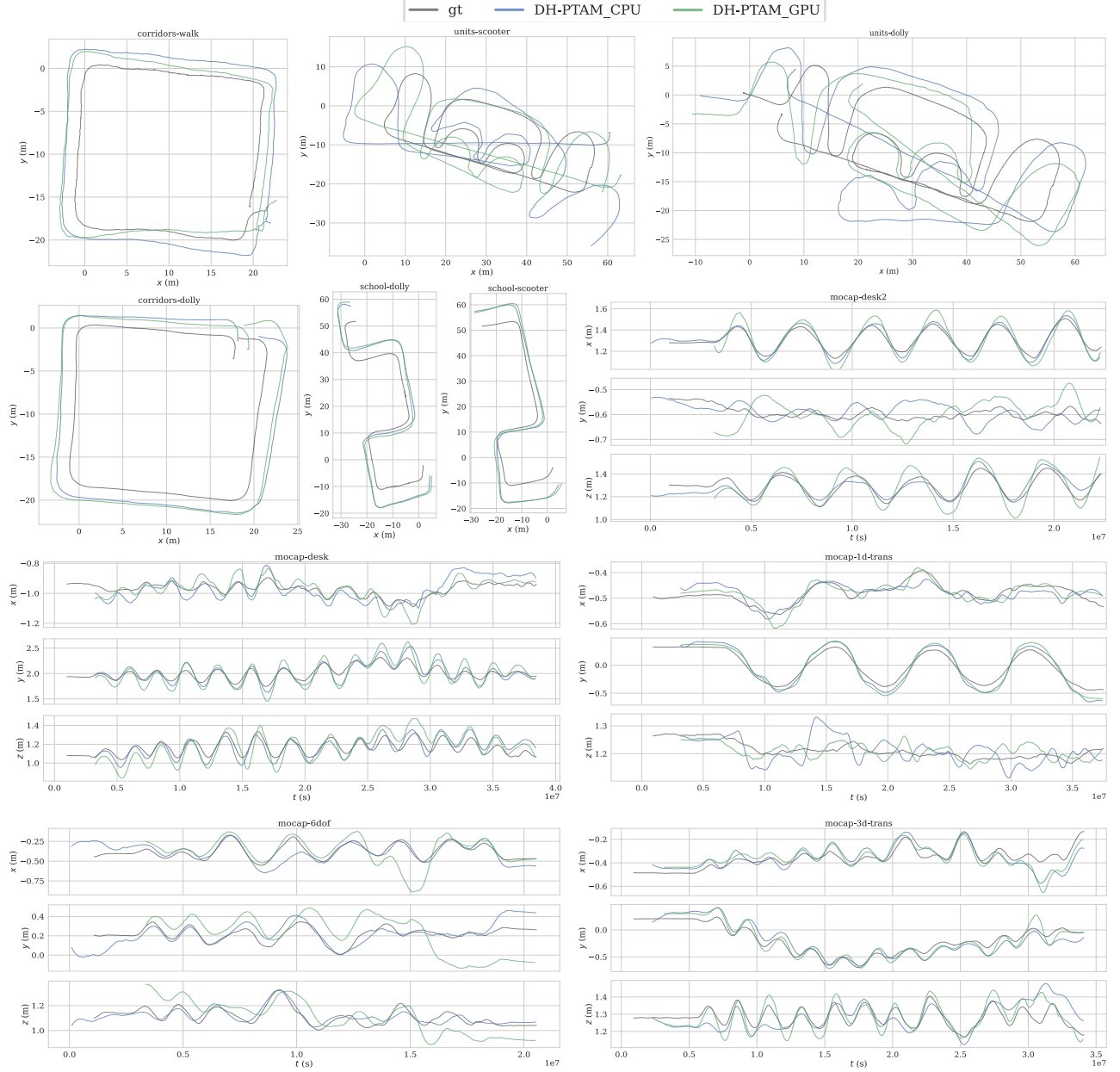


Fig. 7. DH-PTAM (GPU (no events) vs. CPU (event-aided)) qualitative analysis. All trajectories are transformed to a reference frame as the ground truth poses using the extrinsic parameters, followed by an alignment with all poses by Umeyama’s SE(3) method implemented in [32]. Large-scale trajectories show high-quality loop closure detection in the case of R2D2 on GPU. Small-scale trajectories show the high accuracy of the event-aided version of DH-PTAM.

case of units sequences, DH-PTAM could outperform the VLSLAM systems based on the ATE metric. Fig. 7 gives an overview of the high-quality loop detection of DH-PTAM in the case of corridors sequences. Loop detection failure can be noticed only when the RAM overflows while running the system with enormous point clouds, as in the case of units sequences. We provide trajectory smoothing and post-processing script with our open-source implementation to join estimated trajectory increments in case of RAM overflow failures.

#### B. TUM-VIE small-scale experiments

As noticed in [33], the calibrationA (mocap-desk, mocap-desk2) sequences have more accurate depth estimation results

than calibrationB (rest of mocap and TUM-VIE large-scale) sequences due to the significant calibration errors in the latter. Hence, we perform our comparative evaluation on TUM-VIE small-scale (mocap-) sequences using calibrationA parameters. Although the same high-quality calibrationA parameters apply to both desk2 and desk sequences with the same spiral motion, DH-PTAM performs the best with desk2 sequence but the worst with desk sequence. This occurs since the scene of the desk sequence is bounded by a close-by white wall that strict the depth, and hence DH-PTAM front-end detects low quality and fewer features for desk than desk2. Table II shows that the more DoF excited (6dof, desk2) and the consistent loops detection (1d-trans), the better the pose estimation quality.



## V. CONCLUSION

In this paper, we presented the DH-PTAM system for robust parallel tracking and mapping in dynamic environments using stereo images and event streams. The proposed system builds upon the principles of S-PTAM and extends it with a learning-based approach to handle the sparse and noisy nature of event-based sensors while leveraging the rich information provided by fusion frames. Our experiments demonstrate that DH-PTAM outperforms state-of-the-art visual-inertial SLAM methods, particularly in challenging scenarios such as fast motion, HDR, and occlusions. The proposed system can achieve better performance on a GPU and provides a scalable and accurate solution for 3D reconstruction and pose estimation. Future work includes investigating the potential of integrating inertial navigation sensors, such as IMUs, and exploring the integration of additional deep learning components for improving loop-closure robustness and accuracy. DH-PTAM has the potential to provide robust and accurate 3D mapping and localization, which are crucial for the successful operation of long-term navigation systems.

## REFERENCES

- [1] A. Soliman, H. Hadj-Abdelkader, F. Bonardi, S. Bouchafa, and D. Sidibé, "MAV localization in large-scale environments: A decoupled optimization/filtering approach," *Sensors*, vol. 23, no. 1, 2023.
- [2] Z. Xu, Z. Rong, and Y. Wu, "A survey: which features are required for dynamic visual simultaneous localization and mapping?" *Visual Computing for Industry, Biomedicine, and Art*, vol. 4, no. 1, pp. 1–16, 2021.
- [3] Y. Almalioglu, M. Turan, N. Trigoni, and A. Markham, "Deep learning-based robust positioning for all-weather autonomous driving," *Nature Machine Intelligence*, vol. 4, no. 9, pp. 749–760, 2022.
- [4] J. Hidalgo-Carrió, G. Gallego, and D. Scaramuzza, "Event-aided direct sparse odometry," in *Proceedings of the IEEE/CVF Conference on Computer Vision and Pattern Recognition*, 2022, pp. 5781–5790.
- [5] S. Sun, G. Cioffi, C. De Visser, and D. Scaramuzza, "Autonomous quadrotor flight despite rotor failure with onboard vision sensors: Frames vs. events," *IEEE Robotics and Automation Letters*, vol. 6, no. 2, pp. 580–587, 2021.
- [6] D. DeTone, T. Malisiewicz, and A. Rabinovich, "Superpoint: Self-supervised interest point detection and description," in *Proceedings of the IEEE conference on computer vision and pattern recognition workshops*, 2018, pp. 224–236.
- [7] J. Revaud, C. De Souza, M. Humenberger, and P. Weinzaepfel, "R2d2: Reliable and repeatable detector and descriptor," *Advances in neural information processing systems*, vol. 32, 2019.
- [8] L. Gao, Y. Liang, J. Yang, S. Wu, C. Wang, J. Chen, and L. Kneip, "VECTor: A versatile event-centric benchmark for multi-sensor slam," *IEEE Robotics and Automation Letters*, vol. 7, no. 3, pp. 8217–8224, 2022.
- [9] S. Klenk, J. Chui, N. Demmel, and D. Cremers, "Tum-vie: The tum stereo visual-inertial event dataset," in *2021 IEEE/RSJ International Conference on Intelligent Robots and Systems (IROS)*. IEEE, 2021, pp. 8601–8608.
- [10] A. Merzlyakov and S. Macenski, "A comparison of modern general-purpose visual slam approaches," in *2021 IEEE/RSJ International Conference on Intelligent Robots and Systems (IROS)*. IEEE, 2021, pp. 9190–9197.
- [11] Z. Teed and J. Deng, "Droid-slam: Deep visual slam for monocular, stereo, and rgb-d cameras," *Advances in Neural Information Processing Systems*, vol. 34, pp. 16 558–16 569, 2021.
- [12] F. Nie, W. Zhang, Z. Yao, Y. Shi, F. Li, and Q. Huang, "Lcpf: A particle filter lidar slam system with loop detection and correction," *IEEE Access*, vol. 8, pp. 20 401–20 412, 2020.
- [13] R. Jurevičius, V. Marcinkevičius, and J. Šeibokas, "Robust gnss-denied localization for uav using particle filter and visual odometry," *Machine Vision and Applications*, vol. 30, no. 7, pp. 1181–1190, 2019.
- [14] G. Grisetti, R. Kümmerle, C. Stachniss, and W. Burgard, "A tutorial on graph-based slam," *IEEE Intelligent Transportation Systems Magazine*, vol. 2, no. 4, pp. 31–43, 2010.
- [15] C. Campos, R. Elvira, J. J. G. Rodríguez, J. M. Montiel, and J. D. Tardós, "OrbSLAM3: An accurate open-source library for visual, visual-inertial, and multimap slam," *IEEE Transactions on Robotics*, vol. 37, no. 6, pp. 1874–1890, 2021.
- [16] V. Usenko, N. Demmel, D. Schubert, J. Stückler, and D. Cremers, "Visual-inertial mapping with non-linear factor recovery," *IEEE Robotics and Automation Letters*, vol. 5, no. 2, pp. 422–429, 2019.
- [17] T. Qin, J. Pan, S. Cao, and S. Shen, "A general optimization-based framework for local odometry estimation with multiple sensors," *arXiv preprint arXiv:1901.03638*, 2019.
- [18] P. Koniusz, F. Yan, and K. Mikolajczyk, "Comparison of mid-level feature coding approaches and pooling strategies in visual concept detection," *Computer vision and image understanding*, vol. 117, no. 5, pp. 479–492, 2013.
- [19] D. Gálvez-López and J. D. Tardós, "Bags of binary words for fast place recognition in image sequences," *IEEE Transactions on Robotics*, vol. 28, no. 5, pp. 1188–1197, October 2012.
- [20] Z. Ji, F. Wang, X. Gao, L. Xu, and X. Hu, "Ssnet: Learning mid-level image representation using salient superpixel network," *Applied Sciences*, vol. 10, no. 1, 2020.
- [21] H. Rebecq, T. Horstschäfer, G. Gallego, and D. Scaramuzza, "Evo: A geometric approach to event-based 6-dof parallel tracking and mapping in real time," *IEEE Robotics and Automation Letters*, vol. 2, no. 2, pp. 593–600, 2016.
- [22] A. Sironi, M. Brambilla, N. Bourdis, X. Lagorce, and R. Benosman, "Hats: Histograms of averaged time surfaces for robust event-based object classification," in *Proceedings of the IEEE Conference on Computer Vision and Pattern Recognition*, 2018, pp. 1731–1740.
- [23] D. Gehrig, A. Loquercio, K. G. Derpanis, and D. Scaramuzza, "End-to-end learning of representations for asynchronous event-based data," in *Proceedings of the IEEE/CVF International Conference on Computer Vision*, 2019, pp. 5633–5643.
- [24] A. Soliman, F. Bonardi, D. Sidibé, and S. Bouchafa, "IBISCape: A simulated benchmark for multi-modal SLAM systems evaluation in large-scale dynamic environments," *Journal of Intelligent & Robotic Systems*, vol. 106, no. 3, p. 53, Oct 2022.
- [25] D. Gehrig, H. Rebecq, G. Gallego, and D. Scaramuzza, "Eklt: Asynchronous photometric feature tracking using events and frames," *International Journal of Computer Vision*, vol. 128, no. 3, pp. 601–618, 2020.
- [26] A. R. Vidal, H. Rebecq, T. Horstschäfer, and D. Scaramuzza, "Ultimate slam? combining events, images, and imu for robust visual slam in hdr and high-speed scenarios," *IEEE Robotics and Automation Letters*, vol. 3, no. 2, pp. 994–1001, 2018.
- [27] H. Kim, S. Leutenegger, and A. J. Davison, "Real-time 3d reconstruction and 6-dof tracking with an event camera," in *European conference on computer vision*. Springer, 2016, pp. 349–364.
- [28] P. R. G. Cadena, Y. Qian, C. Wang, and M. Yang, "Spade-e2vid: Spatially-adaptive denormalization for event-based video reconstruction," *IEEE Transactions on Image Processing*, vol. 30, pp. 2488–2500, 2021.
- [29] Y. Zhou, G. Gallego, and S. Shen, "Event-based stereo visual odometry," *IEEE Transactions on Robotics*, vol. 37, no. 5, pp. 1433–1450, 2021.
- [30] B. Kueng, E. Mueggler, G. Gallego, and D. Scaramuzza, "Low-latency visual odometry using event-based feature tracks," in *2016 IEEE/RSJ International Conference on Intelligent Robots and Systems (IROS)*. IEEE, 2016, pp. 16–23.
- [31] T. Pire, T. Fischer, G. Castro, P. De Cristóforis, J. Civera, and J. J. Berles, "S-ptam: Stereo parallel tracking and mapping," *Robotics and Autonomous Systems*, vol. 93, pp. 27–42, 2017.
- [32] M. Grupp, "evo: Python package for the evaluation of odometry and slam," Note: <https://github.com/MichaelGrupp/evo>, 2017.
- [33] S. Ghosh and G. Gallego, "Multi-event-camera depth estimation and outlier rejection by refocused events fusion," *Advanced Intelligent Systems*, vol. 4, no. 12, p. 2200221, 2022.